Chaos, Solitons and Fractals 167 (2023) 113122

Contents lists available at ScienceDirect

Chaos, Solitons and Fractals

journal homepage: www.elsevier.com/locate/chaos

The role of the fitness model in the suppression of neuronal synchronous behavior with three-stage switching control in clustered networks

A.S. Reis [a,*], E.L. Brugnago [a], R.L. Viana [b], A.M. Batista [c], K.C. Iarosz [d,e], F.A.S. Ferrari [f,g], I.L. Caldas [a]

[a] Physics Institute, University of São Paulo, 05508-090, São Paulo, SP, Brazil
[b] Department of Physics, Federal University of Paraná, 81531-980, Curitiba, PR, Brazil
[c] Department of Mathematics and Statistics, State University of Ponta Grossa, 84030-900, Ponta Grossa, PR, Brazil
[d] Department of Exact, Natural and Enginnering Centro universitário UNIFATEB, 84266-010, Telêmaco Borba, PR, Brazil
[e] Graduate Program - Chemical Engineering, Federal University of Technology, 84017-220, Ponta Grossa, PR, Brazil
[f] Department of Physics, Federal Technological University of Paraná, 85503-390, Pato Branco, PR, Brazil
[g] Graduate Program in Computational Modeling and Systems, State University of Montes Claros, 39401-089, Montes Claros, MG, Brazil

ARTICLE INFO

Keywords:
Neuronal network
Scale-free
Fitness model
Synchronization
Suppression

ABSTRACT

In this work, we investigate the synchronization of neuronal activity through a model of a clustered network formed by scale-free subnetworks. These simulate the areas of the cerebral cortex and capture the spatial distribution of the vertices. The growth of the scale-free subnetworks takes place according to the fitness model, and the architecture of the clustered network presents internal and external links to simulate connections inside and between cortical areas. The corticocortical connections are established according to a human connectivity matrix obtained through experimental data. The model also considers electrical and chemical synapses. A two-dimensional map, in the bursting regime, simulates the dynamic behavior of the neuron. The high synchronization of neuronal activity is revealed by the Kuramoto order parameter. To corroborate the analyses using the order parameter, we calculate a suppression measure. In order to suppress this synchronization, we propose a three-stage switching control as a function of the delayed mean-field in each subnetwork. This suppressor agent is effective in two scenarios, whether applied according to the spatial distribution of neurons or in the emitting hubs of the subnetworks. Our results show that the fitness model has a relevant role in the study of neuronal activity suppression, allied to the application of a three-stage switching control by means of a time-delayed feedback method being an efficient way to suppress synchronization in clustered networks.

1. Introduction

The investigation of the collective behavior of several systems allows us to understand their emergent behavior, like synchronization, which is a phenomenon present in many real systems [1,2]. Study it has a fundamental role in many fields of knowledge, such as physics, biology, chemistry and medicine [3,4]. It is possible to observe synchronization phenomena in complex networks and, in particular, neuronal network systems [5–7]. The implementation of graphs as a means of simulating neuronal networks has been widely used in recent years [8]. This mathematical resource allows us to optimally build a model of a neuronal network whose architecture of their connections is complex, thus being able to observe the dynamic characteristics associated with these systems [9]. Currently, to study neuronal networks by means of computational simulations, there are models that consider small-world [10,11], scale-free [12–14] and random networks [15].

In general, there is no way of knowing whether the synchronized activities of neurons can cause any damage to the human brain. However, recent studies have indicated that some synchronized neuronal activities, in certain areas of the cortex, can lead to motor dysfunctions such as epilepsy, essential tremors, and Parkinson disease [16–21]. Thus, the study of synchronization in networks of neurons has been of great interest in neuroscience [22], being used mainly to understand synchronization in several systems that consider small-world [23–25] and scale-free networks [26,27], that can be related, in some simulations, to models with connectivity maps [28,29].

Usually, small-world networks are used to simulate a neuronal network. Nevertheless, construction through scale-free networks is also often used for the same purpose. In fact, small-world and scale-free networks are robust and the information considering both topologies can be transferred with efficiency. Heuvel et al. [30] studied

* Corresponding author.
E-mail address: adrianereis@usp.br (A.S. Reis).

https://doi.org/10.1016/j.chaos.2023.113122
Received 15 August 2022; Received in revised form 8 December 2022; Accepted 5 January 2023

small-world and scale-free organization of voxel-based resting-state functional connectivity in the human brain. They showed a possible combined small-world and scale-free organization in the network structure. Still, Eguiluz et al. [31] demonstrated scale-free organization on a voxel scale during the performance of auditory tasks and also reported that the probability of finding a link as a function of distance and the distribution of functional connections, are known to be scale-free.

The scale-free network model often fails due to the fact that it does not consider the dynamic evolution of the acquisition rate of new links in the network. In the primary model, proposed by Barabási–Albert [32], two characteristics are highlighted: growth and preferential attachments, the latter giving rise to highly connected nodes, namely hubs. The "winner-take-all" phenomenon, present in scale-free networks, can be solved by considering a variation of this same model. The fitness model, also known as the Bianconi–Barabási model [33], proposes a modification of the rate of acquisition of new links between pairs of distinct nodes; now each node will be connected according to a probability that depends on its fitness. This modification makes the model more plausible, from the point of view that, in real networks, the connection rate between links is closer to what is proposed in this model. However, in a recent work it was found that for clustered networks with a scale-free type network connection architecture, the hub did not exert significant influence on the synchronization or suppression of the network [26]. In this work, we propose to change the topology of the network, in which still grows through a scale-free network model, however the network obeys the procedure of the fitness model growth. By ensuring that the network has other more connected nodes, we investigate how this influences the synchronization of the network and the application of the phase synchronization suppressor agent.

We study the synchronization phenomena in clustered scale-free networks, in each of which the nodes are spatially distributed. The behavior of neuronal firing is simulated through a two-dimensional map [34] in a burst regime. The constructed network considers the architecture of internal connection (within the cortical regions) and external (corticocortical connections), the composition of the internal and external connections configures what we call a clustered network. The model considers the synaptic signature of neuronal links of an electrical and chemical nature [27]. Corticocortical connections are performed by a human connectivity matrix, obtained through experimental data, which captures the density of neural fibers existing between two distinct cortical areas [35]. Each cortical area is designed as a scale-free network, built according to the fitness model, and composed of Rulkov neurons. The coupling of maps, therefore, is based on a term that considers excitatory and inhibitory neuronal potentials, synapses (electrical or chemical), and an addressing matrix derived from the human connectome, being implemented as a neuronal activation function.

Given the association of neuronal activity synchronization with motor dysfunctions, it is important to carry out a study aimed at suppressing high synchronization. In this sense, we propose a suppressor method to reduce the synchronization in two ways, where the suppressor acts: **(a)** on the network considering its three-dimensional distribution; **(b)** only on the neurons with more outgoing connections. The network phase synchronization is measured by the Kuramoto order parameter [36], being this an excellent tool to assess synchronization in neuronal networks [37]. The reduction of the network synchronized activity is measured by the suppression factor, proposed by Rosenblum and Pikovsky [38,39], whose evaluation is performed by measuring the variance of the mean-field of the network. If the network is synchronized in phase, the activity of neuronal firing generates large amplitude oscillations in the mean-field. Otherwise, if the network is not synchronized in phase, the mean-field exhibits small amplitude oscillations.

This paper is divided as follows. In Section 2, we introduce the methods used in this work, presenting the procedure for building the clustered network together with the implementation of the three-dimensional model. Still in this section, we present the model used to simulate the dynamic behavior of the neuron and the coupled map. The phase synchronization measure and the suppressor agent is also discussed in this section. In Section 3, we present the results of neuronal phase synchronization and the assessment of suppression for the clustered network and for cortical areas. Finally, Section 4 is devoted to our discussions and conclusions.

2. Mathematical modeling and methods

In this section, we describe the process of building the clustered network model. Starting with the Bianconi–Barabási model (used for the construction of subnetworks) until the composition of the clustered network. After, we describe the Rulkov neuron and the coupled map system. Also, we present the methods used to evaluate and suppress the network phase synchronization.

2.1. Network construction

The network model used in this work is a proposal to simulate the connections between neurons and distinct cortical areas [27]. The construction is made considering connections at two levels: internal and external. Fig. 1 illustrates the structure scheme of the clustered network. Cortical areas are represented by the cubes inside each hemisphere of the brain, as shown in Fig. 1(a). Each cortical area (subnetwork) is independently modeled by a scale-free network, built according to the fitness model mechanism presented below. The nodes correspond to neurons, and the edges on the same subnetwork are called internal connections. Additionally, the model simulates a three-dimensional distribution of neurons in the cortical areas and simulates two kinds of synapses (electrical and chemical). The subnetworks are interconnected, as corticocortical connections, forming the clustered network. The edges between nodes of different subnetworks are called external connections.

2.1.1. Implementation of fitness model

The fitness model [33] (also known as Bianconi–Barabási model) derives from a well-established model known as scale-free networks proposed by Barabási–Albert [32]. To incorporate the role of fitness, we assume that preferential attachment is driven by the product of a node's fitness, η in a given distribution $\Xi(\eta)$, and its degree k. Briefly, the implementation of the Bianconi–Barabasi model consists of two stages:

1. Growth: at each time step, a new node u with m connections and fitness η_u is added to the network;
2. Preferential attachment: the probability Π_u of a new node connecting to node u is proportional to the product of the degree's node k_u and its fitness η_u, being

$$\Pi_u = \frac{\eta_u k_u}{\sum_v \eta_v k_v}. \tag{1}$$

As in the Barabási–Albert model, the dependence of Π_u on k_u captures the fact that nodes with higher degree have greater visibility. However, the dependence of Π_u on η_u implies that between two nodes with the same degree, the one with the highest fitness is chosen with greater probability. In this way, Eq. (1) increase a chance of even relatively younger nodes can acquire links faster if they have a higher fitness than other nodes.

In the implementation performed in this study, each subnetwork is made up of $V = 200$ nodes. We adopted $m = 4$ and, for each new vertex (the same as node), the fitness parameter is drawn according to the uniform random distribution on the open unitary interval, i.e. $\eta \in (0, 1)$.

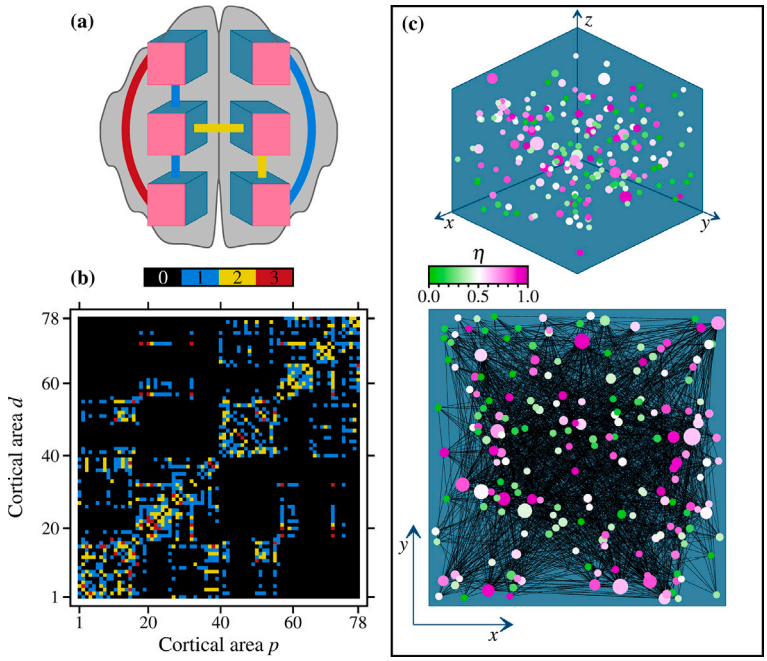

Fig. 1. (a) Representative scheme of clustered network structure. Cortical areas are simulated in cubic regions and interconnected by bundles of corticocortical links. (b) Weighted human connectivity matrix. The colors correspond to the assigned weights: 0 (black), 1 (blue), 2 (yellow) and 3 (red). (c) Cortical areas (subnetworks) are created according to the fitness model with the neurons spatially distributed (top) and, (dawn) projection of the network in 2D for better visualization. The nodes are represented by circles, with the radius being proportional to the degree and the colors representing the fitness η of each one. (For interpretation of the references to color in this figure legend, the reader is referred to the web version of this article.)

2.1.2. Subnetwork spatial distribution and edges orientation

Neurons present within cortical areas are spatially distributed, as shown in the top of Fig. 1(c). The position of vertices is randomly selected in a three-dimensional cubic region with side $2L$, and their location is given in Cartesian coordinates. The random positioning is equiprobable in the three axes, which results in a homogeneous spatial distribution of the vertices. At the bottom of Fig. 1(c), we show a two-dimensional projection of an example subnetwork that gives us an idea of the graph generated through the fitness model. In this illustration, the vertices are represented by circles, whose radius is proportional to their degree, and the fitness is in colors, where $\eta \leq 0.5$ is from green to white and $\eta \geq 0.5$ is from white to magenta.

To simulate the two kinds of synapses, chemical (unidirectional edge) and electrical (bidirectional edge), we consider the Euclidean distance between pairs of connected vertices, reserving the shortest internal connections as electrical. This is an objective criterion that allows us to select the proportion of 10% of electrical connections. It is worth mentioning that, in this model, the type of connection (electrical or chemical) is not randomly selected, but decided as a function of the edge's length. Given a pair of vertices connected by a unidirectional edge in the same subnetwork, it is permanently established which one is the sender (presynaptic neuron) and which one is the receiver (postsynaptic neuron), with a chance of 50% for each direction. Also, since the subnetwork has a directional character, we guarantee that all vertices have at least one input (postsynaptic stance) and one output (presynaptic stance). The bidirectional connection is understood as input and output simultaneously.

For the u-th neuron, from the p-th cortical area, the amount of internal connections in which it is postsynaptic is given by $K_{\mathrm{E/C}}^{(p,u)}$, where E/C identifies the type of link as electrical/chemical. Completely, $\widetilde{K}_{\mathrm{E/C}}^{(p,u)}$ is the amount of internal connections in which the neuron is presynaptic. By construction, every neuron must have at least one input and one output internal connection, so $\forall\ (p,u)$ is worth

$$K^{(p,u)} = K_{\mathrm{E}}^{(p,u)} + K_{\mathrm{C}}^{(p,u)} > 0, \tag{2}$$

$$\widetilde{K}^{(p,u)} = \widetilde{K}_{\mathrm{E}}^{(p,u)} + \widetilde{K}_{\mathrm{C}}^{(p,u)} > 0. \tag{3}$$

Since electrical synapses are bidirectional, is verified $K_{\mathrm{E}}^{(p,u)} = \widetilde{K}_{\mathrm{E}}^{(p,u)}$. Note that the degree of each node in the scale-free network is

$$k^{(p,u)} = K_{\mathrm{E}}^{(p,u)} + K_{\mathrm{C}}^{(p,u)} + \widetilde{K}_{\mathrm{C}}^{(p,u)}. \tag{4}$$

2.1.3. Clustered network model

The external connections are exclusively unidirectional (chemical) and, in the process of building the network, established after the duly created subnetworks. Those links are distributed according to a weighted connectivity matrix $\mathbb{M}$, obtained experimentally from a human connectome data [35] and shown in Fig. 1(b), in which the human cortex is divided into $N = 78$ areas. The weights were established according to the density of neuronal fibers. We define four levels of connectivity, according to weights 0, 1, 2 and 3, as follows (in order): no connection, sparse, moderate and dense connections. Given a pair (p,q) of subnetworks, this is connected by $\delta M^{(p,q)}$ links, where the multiplier $\delta = 18$ and $M^{(p,q)}$ is an element of the matrix $\mathbb{M}$. This means that, in cases where weight 1 is assigned, 18 connections between different cortical areas are established, consequently, for weights 2 and 3; 36 and 54 corticocortical connections are added, respectively. It is important to note that if the assigned weight is 0, no connections are added. The blue, yellow and red lines in Fig. 1(a) represent the amount of connections assigned between two distinct cortical areas, whose weight is according to the color scheme shown in Fig. 1(b).

To generate the external connections, we only consider the elements in the upper triangle of $\mathbb{M}$. One vertex from the subnetwork p and another from the subnetwork q is drawn, in an equiprobable way, without any prior connection between them. The partial adjacency matrices $\mathbb{A}_{\mathrm{E}}^{(p)}$ and $\mathbb{A}_{\mathrm{C}}^{(p,q)}$, respectively for electrical and chemical connections, give us a fully description of the clustered network. Since, in this model, bidirectional edges occur only in internal connections, there is a symmetric matrix $\mathbb{A}_{\mathrm{E}}^{(p)}$ for each subnetwork. The element $A_{\mathrm{E}}^{(p)(u,v)} = 1$ represents an edge connecting the uth and vth vertices of the cortical area p, still $A_{\mathrm{E}}^{(p)(u,v)} = 0$ when there is no link between them. The $\mathbb{A}_{\mathrm{C}}^{(p,q)}$ matrix is non-symmetric and carries information about the directed edges from the subnetworks p to the q ones. In the case of

its element $A_{\mathrm{C}}^{(p,q)(u,v)} = 1$, there is a chemical connection in which the neuron u, in the cortical area p, is presynaptic, while the neuron v, in the cortical area q, is postsynaptic. Completely, $A_{\mathrm{C}}^{(p,q)(u,v)} = 0$ when have no chemical link in the described direction.

The number of links in each vertex is given by

$$K_{\mathrm{E}}^{(p,u)} = \sum_{v=1}^{V} A_{\mathrm{E}}^{(p)(v,u)}, \tag{5}$$

$$K_{\mathrm{C}}^{(p,u)} = \sum_{v=1}^{V} A_{\mathrm{C}}^{(p,p)(v,u)}, \tag{6}$$

$$\tilde{K}_{\mathrm{C}}^{(p,u)} = \sum_{v=1}^{V} A_{\mathrm{C}}^{(p,p)(u,v)}, \tag{7}$$

$$G_{\mathrm{C}}^{(p,u)} = \sum_{q=1}^{N}\sum_{v=1}^{V} A_{\mathrm{C}}^{(q,p)(v,u)}, \tag{8}$$

where $G_{\mathrm{C}}^{(p,u)}$ is the total number of chemical connections in that neuron, being the sum of internal and external connections.

2.2. Neuron mathematical model

2.2.1. Discrete time neuronal model

The dynamic behavior of the neuron is mathematically simulated by a two-dimensional map. The phenomenological model proposed by Rulkov [34] mimics the patterns of neuronal firing, being represented as follows:

$$x_{n+1} = f(\alpha, x_n, y_n), \tag{9}$$

$$y_{n+1} = y_n - \sigma(x_n - \rho), \tag{10}$$

where $f(\alpha, x_n, y_n) = \alpha/(1 + x_n^2) + y_n$. The fast variable of the map (x_n) simulates the neuronal membrane potential, while the slow variable (y_n) has no biological meaning assigned. For this work we use the typical values that characterize bursts regime: $\alpha \in [4.1, 4.2)$, $\sigma = 10^{-3}$ and $\rho = -1.0$.

2.2.2. Coupled map

The neuronal network model is established by including coupling terms in the Eq. (9) of the Rulkov map. The different types of connections between neurons, electrical and chemical links, are modeled by additive terms and described separately. Since the network is structured as a cluster of subnetworks, the maps (neurons) are identified by a superscript pair of indexes (p, u), which p (from portion) indicates the cortical area and u (from unit) corresponds to a neuron within it. So, the coupled map is described as

$$x_{n+1}^{(p,u)} = f\left(\alpha^{(p,u)}, x_n^{(p,u)}, y_n^{(p,u)}\right) + \varepsilon_{\mathrm{E}}\mathscr{C}_{\mathrm{E}}^{(p,u)} + \varepsilon_{\mathrm{C}}\mathscr{C}_{\mathrm{C}}^{(p,u)}, \tag{11}$$

where $\varepsilon_{\mathrm{E/C}}$ is the electrical/chemical coupling strength and $\mathscr{C}_{\mathrm{E/C}}^{(p,u)}$ is the electrical/chemical coupling factor dependent on the connections to which the neuron is postsynaptic. Neuronal diversity is simulated by means of the random assignment of $\alpha^{(p,u)} \in [4.1, 4.2)$, being drawn a value of this parameter, in an equiprobable distribution, for each map (p, u).

The implemented electrical coupling factor is given by

$$\mathscr{C}_{\mathrm{E}}^{(p,u)} = \begin{cases} 0, \text{ if } K_{\mathrm{E}}^{(p,u)} = 0; \\ \dfrac{\sum_{v=1}^{V} A_{\mathrm{E}}^{(p)(v,u)}\left(x_n^{(p,v)} - x_n^{(p,u)}\right)}{K_{\mathrm{E}}^{(p,u)}}, \text{ otherwise.} \end{cases} \tag{12}$$

Similarly, the chemical coupling factor is

$$\mathscr{C}_{\mathrm{C}}^{(p,u)} = \quad = \begin{cases} 0, \text{ if } G_{\mathrm{C}}^{(p,u)} = 0; \\ \dfrac{\sum_{q=1}^{N}\sum_{v=1}^{V} A_{\mathrm{C}}^{(q,p)(v,u)} W_n^{(q,p)(v,u)}}{G_{\mathrm{C}}^{(p,u)}}, \text{ otherwise.} \end{cases} \tag{13}$$

Where

$$W_n^{(q,p)(v,u)} = \left(M^{(q,p)} + \delta_{qp}\right)\mathscr{H}\left(x_n^{(q,v)} - \theta\right)\left(P^{(q,v)} - x_n^{(p,u)}\right). \tag{14}$$

Note that N is the amount of cortical areas presented in the human connectome, and V is the number of vertices in each subnetwork. Here, $\mathscr{H}$ is the Heaviside function, which is the neuronal activation function in this model. The neuronal potential $P^{(p,u)}$ can be inhibitory ($P^{(p,u)} = -0.5$) or excitatory ($P^{(p,u)} = 1.0$). We configure the subnetwork so that neurons are 20% inhibitory and 80% excitatory [40]. Still in Eq. (14), the threshold potential $\theta = -1.0$ and the term δ_{qp} is the delta of Kronecker used to assign weight 1 to internal connections in the subnetwork. So, internal connections in each subnetwork have unitary weight, while links between different subnetworks have weights according to the matrix $\mathbb{M}$.

2.3. Neuronal phase synchronization

2.3.1. Kuramoto order parameter

The network synchronization is evaluated through the Kuramoto order parameter [36]. Originally proposed by Winfree [41], and later adapted by Kuramoto, this model was developed to study the phase synchronization of a set of coupled oscillators. The system phase synchronization level is measured by a order parameter which is between 1 (fully synchronized) and 0 (fully desynchronized). Similarly, we can use the same principle to assess the synchronization of burst neurons. After coupling the network (acc. Section 2.2.2), and the due adjustment of the synaptic intensity parameters is made, the neurons begin to fire at the same time, causing their phases to be synchronized.

The phase of neurons is given by the relation of the fast and slow variables of the Rulkov map. In this model, each start (end) of a burst in the fast variable corresponds to a maximum (minimum) in the time series of the slow variable. Through this association, we can define a geometric phase in the interval of $[0,2\pi)$ as

$$\varphi_n^{(p,u)} := 2\pi\frac{n - t_k^{(p,u)}}{t_{k+1}^{(p,u)} - t_k^{(p,u)}}, \tag{15}$$

where t_k is the instant at which the kth burst starts. Defined in this way, the phase $\varphi_n^{(p,u)}$, associated with neuron u in the cortical area p, increases monotonically between the discrete time instants t_k and t_{k+1}, with $t_k \le n < t_{k+1}$. The average time of phase synchronization for the clustered network is given by

$$R = \frac{1}{(\Delta+1)}\sum_{n=n_a}^{n_a+\Delta}\frac{1}{NV}\left|\sum_{p=1}^{N}\sum_{u=1}^{V} e^{i\varphi_n^{(p,u)}}\right|, \tag{16}$$

where $\Delta + 1 = 5\times10^3$ is the number of iterations taken into account for the average and n_a is the start time sample after the transient. In the same way, the phase synchronization of neuronal bursts in each cortical area is calculated by the equation

$$R^{(p)} = \frac{1}{(\Delta+1)}\sum_{n=n_a}^{n_a+\Delta}\frac{1}{V}\left|\sum_{u=1}^{V} e^{i\varphi_n^{(p,u)}}\right|. \tag{17}$$

Note that, in general, $R \neq N^{-1}\sum_{p=1}^{N} R^{(p)}$.

2.4. Time-delayed feedback

Originally, the method proposed by Pyragas [42], to suppress the synchronization, uses a control obtained from the difference between the current state of the system and one delayed by a periodic unstable orbit. Here, we propose as a synchronization suppressor agent a perturbation g as a function of the delayed mean-field $X_{n-\tau}^{(p)}$ of each subnetwork. The mean-field $X_n^{(p)}$ of the cortical area p in the n interaction is

$$X_n^{(p)} := \frac{1}{V}\sum_{u=1}^{V} x_n^{(p,u)}. \tag{18}$$

In the numerical application, a delay τ is considered between the computation of the mean-field and the disturbance as a function of it. Additionally, it is plausible to consider a perturbation weighting according to the two main characteristics of the subnetworks that model the cortical areas in this study: **(a)** Vertices are spatially homogeneously distributed in a finite region and **(b)** are connected forming a scale-free network. Thus, we employ a local weighter $\beta^{(p,u)}$ consisting of a weight dependent on the position of neurons in each cortical area or their connectivity. The Eq. (11), which simulates the neuronal membrane potential in coupled form, is modified by addition of a feedback term, and becomes

$$x_{n+1}^{(p,u)} = f\left(\alpha^{(p,u)}, x_n^{(p,u)}, y_n^{(p,u)}\right) + \varepsilon_{\mathrm{E}}\mathscr{C}_{\mathrm{E}}^{(p,u)} + \varepsilon_{\mathrm{C}}\mathscr{C}_{\mathrm{C}}^{(p,u)} + \\ + \varepsilon_{\mathrm{F}}\beta^{(p,u)} g\left(X_{n-\tau}^{(p)}\right), \tag{19}$$

where ε_{F} is the feedback strength and we defined the suppressor agent g as a three-stage switching controller.

2.4.1. Three-stage switching control

The perturbation added in the Eq. (19), to suppress the phase synchronization of the network, consists of applying a signal that responds in three different ranges of the delayed mean-field values of each subnetwork. This method of switched control allows the existence of a non-active range, where $g = 0$, as well as two others intervals with different responses. The piecewise function that describes the behavior of the suppressor agent is

$$g\left(X_{n-\tau}^{(p)}\right) = \begin{cases} 1, \text{ if } X_{n-\tau}^{(p)} < \gamma_1; \\ 0, \text{ if } \gamma_1 \le X_{n-\tau}^{(p)} < \gamma_2; \\ -1, \text{ if } \gamma_2 \le X_{n-\tau}^{(p)}; \end{cases} \tag{20}$$

This function presents an undisturbed interval $\gamma_1 \le X_{n-\tau}^{(p)} < \gamma_2$, whose choice of boundary values $\gamma_1 = -1.25$ and $\gamma_2 = \theta$ entails not disturbing the cortical area p if it is desynchronized. In the case where the firing bursts of the neurons of the subnetwork are phase synchronized, the mean-field presents oscillations below and above the values adopted for γ_1 and γ_2, respectively. Thus, the proposed perturbation acts by stimulating firings when the mean-field corresponds to most neurons in the quiescent stage, as well as inhibiting firings when most of them are in an active burst.

2.4.2. Local weighter

We include the weight $\beta^{(p,u)}$ in the feedback term in order to take into account specificities present in the subnetworks, such as the spatial distribution of neurons (exploring the characteristic **a**) or their connectivity (related to the characteristic **b**).

In the spatial approach, we employ a local weighter as a function of the Euclidean distance $d^{(p,u)}$ from each vertex to the geometric center $\mathscr{O}^{(p)}$ of the cubic region in which p subnetwork is distributed, where this cubic region has side $2L$ and $0 \le d^{(p,u)} \le \sqrt{3}L$. We propose the application of the suppressor agent in Q concentric spherical shells centered on $\mathscr{O}^{(p)}$, whose radii are

$$r_{\mathrm{in}}^{(q)} = \frac{(q-1)L}{Q} \quad \text{(inner radius)}, \tag{21}$$

$$r_{\mathrm{out}}^{(q)} = \frac{qL}{Q} \quad \text{(outer radius)}, \tag{22}$$

with $Q \ge q \in \mathbb{Z}^+$. The local weighter is constant within each shell and falls linearly with increasing q, being zero outside the last spherical region. We define

$$\beta^{(p,u)} = \beta_{\mathrm{a}}^{(p,u)} := \begin{cases} 1 - \dfrac{q-1}{Q}, \text{ for } r_{\mathrm{in}}^{(q)} \le d^{(p,u)} < r_{\mathrm{out}}^{(q)}, \\ 0, \text{ if } r_{\mathrm{out}}^{(Q)} \le d^{(p,u)}. \end{cases} \tag{23}$$

In the subnetwork topology approach (considering the characteristic **b**), we applied the suppressor agent only to neurons with more presynaptic connections in each cortical area, called emission hubs (EHs). Unlike what happens with a primary scale-free model (Barabási–Albert conceptualization), the subnetwork does not have only one hub. In fact, the premise of the fitness model, applied here, is that, during network growth, new nodes in the network also influence connectivity. So, for every p subnetwork, we get a $\mathscr{L}_Q^{(p)}$ list of Q EHs, which can be obtained by a recursive process of vertex selection. Let $\mathscr{U}^{(p)}$ be the set of vertices (p,u) components of the subnetwork p, we can identify (p,u_j) the vertex whose index u_j is the smallest u that maximizes $\widetilde{K}^{(p,u)}$, with $(p,u) \in \mathscr{U}^{(p)} \setminus \mathscr{L}_{j-1}^{(p)}$. In this way, we define

$$\mathscr{L}_0^{(p)} := \emptyset, \ \mathscr{L}_j^{(p)} := \left\{(p,u_j)\right\} \cup \mathscr{L}_{j-1}^{(p)}, \tag{24}$$

where $Q \ge j \in \mathbb{Z}^+$. So, the local weighter is given by the follow definition

$$\beta^{(p,u)} = \beta_{\mathrm{b}}^{(p,u)} := \begin{cases} 1, \text{ if } (p,u) \in \mathscr{L}_Q^{(p)}, \\ 0, \text{ else.} \end{cases} \tag{25}$$

2.4.3. Suppression measure

In addition to the analysis of the order parameter, given by Eq. (16), we calculate the suppression measure S, defined by [38]

$$S := \sqrt{\frac{\mathrm{Var}\left(X_n\right)_{\varepsilon_{\mathrm{F}}=0}}{\mathrm{Var}\left(X_n\right)_{\varepsilon_{\mathrm{F}}}}}, \tag{26}$$

where X_n is the clustered network mean-field in the iteration n, given by

$$X_n := \frac{1}{N}\sum_{p=1}^{N} X_n^{(p)}. \tag{27}$$

The variance $\mathrm{Var}\left(X_n\right)_{\varepsilon_{\mathrm{F}}}$ is calculated over the mean-field samples set $\left\{X_n : n_a \le n \le n_a + \Delta\right\}$ and the subindex ε_{F} indicates the feedback strength adopted in Eq. (19).

The amplitude variation of the mean-field oscillations makes it possible to assess whether, or not, the network is synchronized. What is desired is that the variance of the network disturbed by the feedback term is as small as possible. In fact, the condition that evaluates the success of the employed strategy is satisfied when $S \gg 1$ [39].

3. Results and discussion

All results presented in this paper are obtained under an average of 20 randomly assigned initial conditions. At each initialization, new values of $\alpha^{(p,u)}$ were drawn. The parameter axis are discretized into 21 equidistant values. When not mentioned, we adopt $\varepsilon_{\mathrm{E}} = \varepsilon_{\mathrm{C}} = 0.1$.

3.1. Phase synchronization

The Kuramoto order parameter is calculated for the clustered network and for the cortical areas, shown in Fig. 2. Here, the neuronal network is described according to Eq. (11), i.e. without the feedback disturbance. Combinations in the $\varepsilon_{\mathrm{E}} \times \varepsilon_{\mathrm{C}}$ parameter plane presents low synchronization for $\varepsilon_{\mathrm{C}} \le 0.2$. As the chemical coupling strengths increase, the time average of Kuramoto order parameter grows fast, keeping the clustered network phase synchronization about $R \approx 0.8$, as can be seen in color code in Fig. 2(a). Note that for $\varepsilon_{\mathrm{C}} \approx 0.04$ and greater, R increases slightly with ε_{E}, getting at $R \approx 0.85$. When investigating the phase synchronization on the cortical areas, as illustrated in panel (b), we initially notice a modest increase in the measure of the local synchronization. However, by increasing the strength of chemical synapse, ε_{C}, a transition to the synchronized state is observed. In this case, although the transition is smoother, compared to what occurs in the case of the clustered network, the abrupt growth of the Kuramoto order parameter is still evident. It is noteworthy that for the adopted

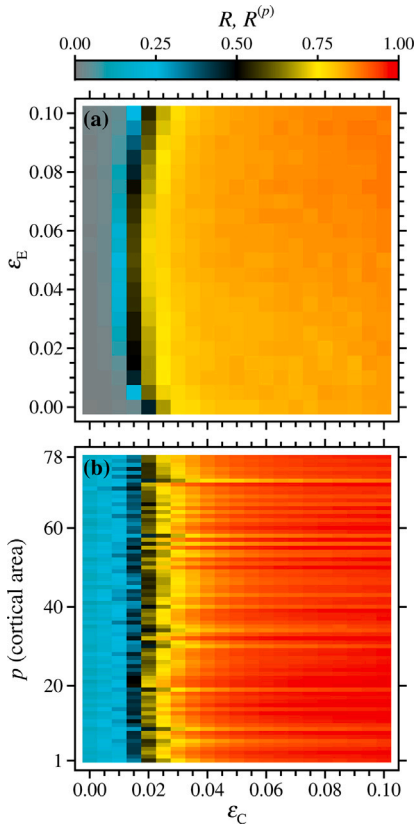

Fig. 2. Time average of Kuramoto order parameter for the neuronal network without feedback disturbance. Synchronization level according to color code. (a) R in the plane $\varepsilon_E \times \varepsilon_C$ for clustered network. Synchronization emerges ($R > 0.5$) for $\varepsilon_C \approx 0.02$, where $R \approx 0.85$ for $\varepsilon_E = \varepsilon_C = 0.1$. (b) $R^{(p)}$ detailed for cortical areas, with $\varepsilon_E = 0.1$ and varying ε_C. In general, subnetworks have higher synchronization levels than the clustered network. (For interpretation of the references to color in this figure legend, the reader is referred to the web version of this article.)

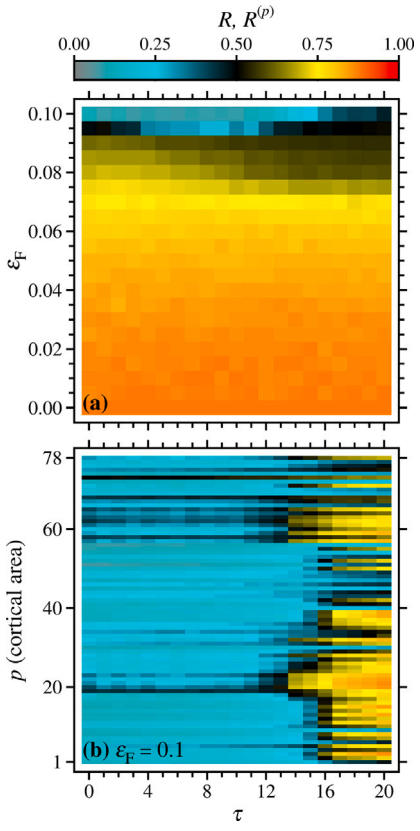

Fig. 3. Neuronal phase synchronization under application of suppressor agent acc. spatial approach. (a) Clustered network synchronization in the $\varepsilon_F \times \tau$ plane. R reaches lower values as ε_F approaches 0.1. (b) Subnetworks synchronization values with $\varepsilon_F = 0.1$. $R^{(p)}$ decreases across all subnetworks to $\tau \approx 14$.. For $\tau > 14$, there are moderate and high synchronized regions. (For interpretation of the references to color in this figure legend, the reader is referred to the web version of this article.)

coupling strength, the neurons preserve the burst behavior both for the network in synchronized and unsynchronized states.

As we see, the synchronization in the cortical areas is greater than for the clustered network. This feature has already been shown in previous works, and is independent of the graph model adopted to build the subnetworks [26,27]. In fact, this abrupt growth is an expected behavior since synchronization is a phenomenon that appears suddenly in dynamical systems, revealing a first-order phase transition characteristic [43].

3.2. Suppressing neuronal phase synchronization

One of the main desires when studying phase synchronization in neuronal networks is to find an efficient method that can be used to suppress high synchronization levels. The synchronization of neuronal firings may be associated with motor dysfunctions. In the following subsections we present some cases in which we use the time-delayed feedback technique combined with the application of a three-stage control in order to suppress synchronization.

3.2.1. Application of the spatial model synchronization suppressor

Given the three-dimensional distribution of the vertices in the simulated cortical areas, we evaluate the performance of the suppressor agent both, in the clustered network and in the subnetworks, according to approach **(a)** described in the Section 2.4.2. Thus, in this topic we show the results for $\beta^{(p,u)} = \beta_a^{(p,u)}$, defined in Eq. (23), with $Q = 4$ concentric spherical regions of action of the suppressor agent.

Although we have not, at this point, evaluated the efficiency of the suppression method by measuring the mean-field variance, with and without feedback control, we can infer whether the suppressor agent used is well employed to suppress network synchronization, by the time average Kuramoto order parameter. The closer the value of R is to 0, the lower the network phase synchronization, that is, the method is employed successfully to suppress the synchronization. In Fig. 3, we present the performance of the suppressor agent in the clustered network, and in the cortical areas, for combinations of ε_F and τ values in Eq. (19). The time average of Kuramoto order parameter reveals high synchronization over a wide region of the plane $\varepsilon_F \times \tau$ (from red to yellow), as shown in panel (a). By varying the value of ε_F from 0 to ≈ 0.08 the network remains strongly synchronized. When $\varepsilon_F > 0.09$, a small region of low synchronization (from gray to cyan) appears, becoming more pronounced when $\varepsilon_F = 0.1$, where the synchronization reaches its lowest value. In panel (b), we set $\varepsilon_F = 0.1$ and analyze the phase synchronization $R^{(p)}$ on the subnetworks. The lowest level of synchronization is achieved for a wide range $0 \leq \tau < 14$. However, there are certain values τ in this interval, for which some subnetworks reaches synchronization has a moderate value $R \approx 0.5$ (black strips), which invade regions of low synchronization (cyan). For some regions, from $\tau = 14$ the phase synchronization increases to $R^{(p)} \approx 0.75$. It is worth highlighting that there are still well-synchronized regions, for $14 < \tau \leq 20$, in cortical areas from 1 to 40, approximately (yellow). Within some of these ranges, the synchronization is even higher, reaching $R^{(p)} \approx 0.8$ (orange).

Since the adopted parameters of coupling strength ($\varepsilon_E = \varepsilon_C = 0.1$) lead to high phase synchronization levels, as seen in Section 3.1, where

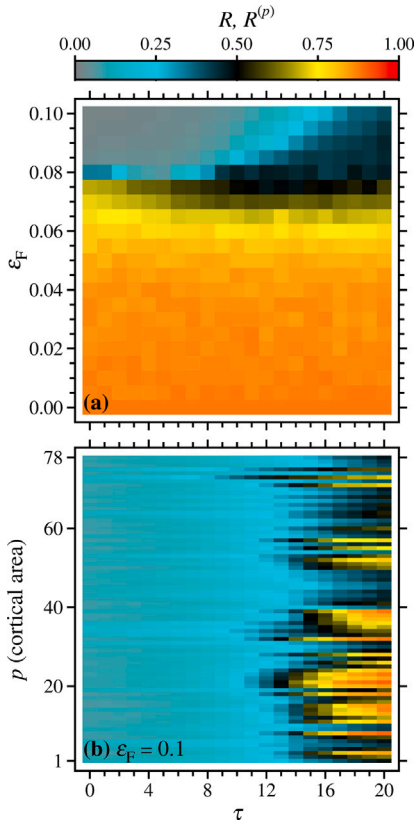

Fig. 4. Phase synchronization values with $Q = 10$ disturbed EHs. (a) R in the plane $\varepsilon_F \times \tau$. the lowest synchronization are achieved when $0.07 \leq \varepsilon_F \leq 0.1$. For $\varepsilon_F < 0.07$, the clustered network is tightly synchronized. (b) $R^{(p)}$ for cortical areas with $\varepsilon_F = 0.1$. Low synchronization seen in cyan. As the value of τ increases, some cortical areas remain moderate synchronization (yellow to orange). (For interpretation of the references to color in this figure legend, the reader is referred to the web version of this article.)

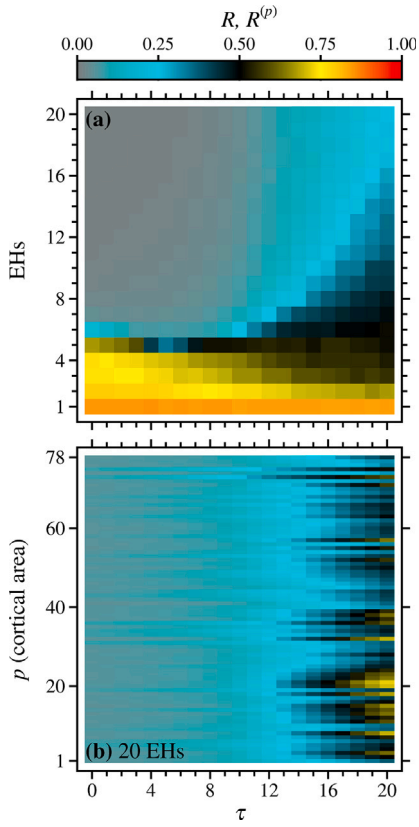

Fig. 5. Investigation of the number of Q disturbed EHs in the phase synchronization decrease. (a) Low synchronization is achieved with $Q > 5$ (gray to cyan) for distinct τ values. (b) For cortical areas, the synchronization remains low for almost all values considered for τ. Only when $\tau > 17$ some subnetworks remains with moderate synchronization (yellow bands). (For interpretation of the references to color in this figure legend, the reader is referred to the web version of this article.)

is observed for the clustered network $R \approx 0.8$ and, for the subnetworks, the majority values $R^{(p)} > 0.95$. The application of suppressor agent give us a significant reduction in synchronization levels, with $\varepsilon_F = 0.1$ and $\tau < 14$ both in the evaluation for the clustered network and for the individual subnetworks. Also satisfactory low values of R are achieved with $\varepsilon_F = 0.09$ and $4 \leq \tau \leq 12$.

3.2.2. Synchronization suppressor applied only in EHs

In this topic we evaluate the synchronization of the network under the action of the suppressor agent according to approach **(b)**, where $\beta^{(p,u)} = \beta_b^{(p,u)}$ defined in Eq. (25). We do this in two ways: first, we define $Q = 10$ EHs and calculate network phase synchronization for combinations of ε_F and τ; in the second way, we set $\varepsilon_F = 0.1$ and obtain the synchronization values varying Q EHs and τ.

In the first case (Fig. 4), we applied the three-stage switching control, acc. Section 2.4.1 Eq. (20), in the 10 EHs of each subnetwork. In panel (a), we present R values in the plane $\varepsilon_F \times \tau$, which reveals high synchronization (from yellow to red) for all values considered from τ and $0 \leq \varepsilon_F \leq 0.07$. The phase synchronization reaches low values for $\varepsilon_F \geq 0.08$ until $\varepsilon_F = 0.1$ (maximum adopted value). When ε_F reaches its maximum value, the measure of clustered network synchronization presents values of $R \approx 0.25$ or less, evidencing the vanishment of the high synchronization. When evaluating the subnetworks individually, the order parameter for $\varepsilon_F = 0.1$, shown in panel (b), reveals low local phase synchronization until $\tau = 12$. As the τ value increases, the plane $p \times \tau$ presents regions with moderate synchronization values, being more synchronized for basically the same cortical areas shown in Fig. 3(b).

In the second case (Fig. 5), we investigate the role of the number of EHs considered for the application of three-stage switching control. What we want to know at this point is how the number of EHs influences the phase synchronization of the system. Is applying control to just 10 EHs enough to suppress synchronization? Are there a minimum number of EHs where, when applying the control, the suppression effects are satisfactory?

Fig. 5(a) shows the synchronization of clustered network for various combinations of the amount Q of EHs and time delay values. The synchronization evaluation reveals a wide region of low synchronization, with $R < 0.5$, when $Q > 5$ EHs (from gray to cyan) with $0 \leq \tau \leq 20$. As the number of disturbed EHs decreases, the clustered network synchronization increases (from yellow to orange) regardless of the value set for τ. Also in panel (a), we have the presence of an intermediate region starting from $\tau = 7$, in which the synchronization presents intermediate values with $R \approx 0.5$, indicating that the network is partially synchronized (black region). The best combination is given considering more than 6 EHs with $0 \leq \tau \leq 9$ (predominantly gray region) for which $R \approx 0$, which indicates that the synchronized activities were suppressed. At the cortical areas, panel (b), the phase synchronization remains low for almost every $p \times \tau$ plane. However, when $\tau > 17$ there are some cortical areas that present high synchronization (yellow region), although less accentuated than observed in Fig. 4(b). These results may suggest that the graph construction architecture for cortical areas has a relevant impact on the suppression of synchronized neuron activities.

3.3. Evaluation by the suppression measure

Although the measurement of Kuramoto order parameter gives us a general idea of what is happening in the system, it is necessary

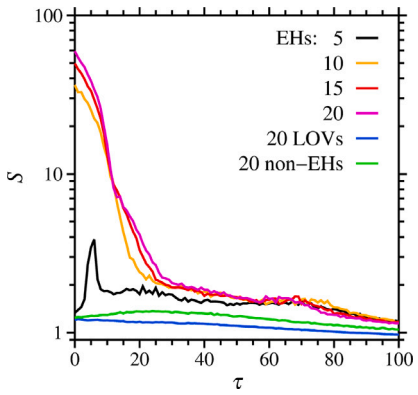

Fig. 6. Suppression measure calculate for the clustered network. Results obtained with $\epsilon_F = 0.1$. Suppression does not have relevant values when considering 5 EHs (black), 20 LOVs and 20 non-EHs. For disturbed EHs equals to 10 (orange), 15 (red) and 20 (magenta), small values of τ result in a suppression measure $S \approx 60$, which indicates that neuronal activity are no phase synchronized. (For interpretation of the references to color in this figure legend, the reader is referred to the web version of this article.)

to quantify the network synchronization drop values in order to corroborate the results presented so far. In this way, we directly assess the suppression of network synchronization when under the effect of feedback perturbation. The suppression of synchronization in the network will be best evaluated accordingly to the suppression measure.

Once it was verified that the most significant reduction in the phase synchronization levels was obtained with the suppressor agent being applied according to the approach **(b)**, where Q EHs are disturbed by the three-stage switching control, we calculated the synchronization suppression measure for different amounts of disturbed EHs, with $\epsilon_F = 0.1$ and varying the time delay τ. We also performed comparisons with two other applications, where the suppressor agent was considered not in the EHs, but in neurons that are not. The suppression measure S is calculated according to definition given in Eq. (26) and the results are shown in Fig. 6. When $Q = 5$ disturbed EHs we verify $S < 10$ (black line) for $0 \leq \tau \leq 100$. Since we want to satisfy the condition $S \gg 1$, for this case, the suppression is still considered small, indicating that neuronal activities are well synchronized. Corroborating the results presented in Fig. 5 discussed in Section 3.2.2. As we increase the number of disturbed EHs, for $\tau \leq 10$ the suppression also grows, getting around $S \approx 36$ (orange line), $S \approx 50$ (red line) and $S \approx 60$ (magenta line) which correspond, respectively at 10,15 and 20 EHs. For $\tau > 10$ the suppression starts to drop quickly, taking the system from the desynchronized to the synchronized state, and this behavior is observed for all the number of evaluated disturbed EHs. In these cases, the best range of values for S is comprised in $0 \leq \tau \leq 12$.

In order to verify the relevance of the EHs to the action of the suppressor agent, we compared it with two other similar forms of application of the three-stage switching control. In the first one, we define a list of the 20 Less Output Vertices (LOVs), which are defined similarly to the EHs, however, instead of maximizing $\widetilde{K}^{(p,u)}$, for the LOVs it is minimized the number of outgoing connections. In the second variation, we apply the suppressor agent on 20 randomly chosen vertices in each subnetwork, which are absent from the list $\mathscr{L}_{20}^{(p)}$, that is, none of these is one of the 20 EHs and we call these non-EHs. In Fig. 6, the blue line represents S obtained with 20 LOVs and the green line identifies the result obtained for 20 non-EHs. In both cases, suppression is observed to be very low, being $S \approx 1$, even for small values of τ. The results of this investigation lead us to state that for the type of model used in the construction of the subnetworks, the EHs play a fundamental role in breaking the neuronal activity phase synchronization.

4. Conclusion

The Barabási–Albert model is designed to capture the mechanisms responsible for the emergence of the scale-free property. Consequently, it has several well-known limitations that have inspired several researches, clarifying the role of the numerous elementary processes that influence the network topology. In this work we explore the phase synchronization in neuronal clustered network, in which the cortical areas are constructed according to the Bianconi–Barabási model and the connections between them are performed by a human connectivity map. The proposed model considers chemical and electrical synaptic connections, with the latter being implemented according to the spatial position of neurons in the simulated cortical areas. The phase synchronization is calculated by the Kuramoto order parameter for the clustered network and for the cortical areas.

Through the calculation of the Kuramoto order parameter, the collective behavior of the system is observed, showing high global and local synchronization, with the latter being slightly higher than the former. This behavior is expected, as the same result was observed other times in neuronal clustered networks. The increase in electrical and chemical synaptic coupling strength contribute to the phase synchronization in our model. Since the model simulates a three-dimensional distribution of the vertices in the subnetworks, we proposed a spatially dependent suppressor agent. In this way, we obtained a reduction in the synchronization of neuronal activity, this suppression method is effective with the feedback strength equal to the coupling strength adopted in the simulations. However, such application leads to a considerable portion of the network under the direct action of the suppressor agent. So, we proposed a second approach based on the existence of hubs in the scale-free network. Specifically, the application of the suppressor agent exclusively to EHs proved to be sufficient to guarantee low phase synchronization of neuronal activity.

It is noteworthy that the three-stage switching control has two active bands, stimulating neuronal firings in cortical regions with average activity below a threshold and inhibiting them in those with activity above the firing threshold. The two stages are observed in subnetworks with phase synchronized activity. The non-active step occurs when the neurons of a cortical area are not synchronized. This characteristic of the proposed suppressor agent, when associated with small delays in the mean-field feedback, leads the Kuramoto order parameter to assume values close to zero, both for the clustered network and for each subnetwork.

We observe that disturbance of less than 5 EHs on each subnetwork is not enough to achieve low synchronization. The measure of suppression by the mean-field, with and with the control, is evaluated in order to corroborate the previous results. The suppression measure is calculated for the control applied to $5, 10, 15$ and 20 EHs. In these cases, the best results occur for more than 10 disturbed EHs, In answer to the questions: What happens if (a) we apply control to vertices with less output connections?; (b) the control is applied to 20 neurons chosen at random, which are not EHs? The answer to both questions highlights the importance of considering a model with aptitude for the proposed model. Considering the fitness model, applying control to specific targets in the network significantly reduces the synchronization of neuronal firings. However, in this work, we do not investigate whether there is a limit on the number of hubs in which applying time-delayed feedback would affect the synchronization reduction. Another important aspect that we do not address here is the question of permanence, that is, for how long can we maintain low synchronization. Studying these aspects in the future opens the way for a better use and robustness of the proposed model.

The results obtained so far may suggest that the graph construction architecture for cortical areas has a relevant impact on the suppression of synchronized neuron activities. Although there is topological influence of the network, synchronization suppression may also have occurred due to the type of control applied to the network. In summary,

our results showed that the graph topology used for the simulation of cortical areas plays a very important role in suppressing network synchronization. Contrary to what was expected, by the results of previous works with a primary scale-free model [27], when using the fitness model, applying the suppressor agent in the hubs causes the synchronization inside the cortical areas to assume low values. This result is interesting due to the fact it allows us to apply suppression control only on strategic targets within each cortical area. This is very relevant given that the area affected by an external electrical stimulus is expected to be as small as possible. In this way, finding neurons with more connections becomes an essential task for the success of this model.

Code availability

The code that support this study is available by request from the corresponding or second author upon reasonable request.

CRediT authorship contribution statement

A.S. Reis: Conceptualization, Methodology, Software, Data curation, Writing – original draft, Visualization, Investigation. **E.L. Brugnago:** Conceptualization, Methodology, Software, Data curation, Writing – original draft, Visualization, Investigation, Validation. **R.L. Viana:** Conceptualization, Methodology, Writing – original draft, Supervision. **A.M. Batista:** Methodology, Writing – original draft. **K.C. Iarosz:** Methodology, Writing – original draft. **F.A.S. Ferrari:** Methodology, Writing – original draft. **I.L. Caldas:** Conceptualization, Methodology, Writing – original draft, Supervision, Resources.

Declaration of competing interest

The authors declare that they have no known competing financial interests or personal relationships that could have appeared to influence the work reported in this paper.

Data availability

Data will be made available on request.

Acknowledgments

Funding

This work was supported by the following agencies: Brazilian National Council for Scientific and Technological Development (CNPq) under Grant Nos. 161949/2020-7; 407299/2018-1; 403120/2021-7; 301019/2019-3. São Paulo Research Foundation (FAPESP) under Grant Nos. 2021/12232-0; 2018/03211-6; 2022/04251-7 and Coordination of Superior Level Staff Improvement (CAPES) under grant 88881.143103/2017-01.

References

[1] Strogatz S. Sync, 1st ed. New York: Theia; 2003.
[2] Acebrón JA, Bonilla LL, Vicente CJP, Ritort F, Spigler R. The Kuramoto model: A simple paradigm for synchronization phenomena. Rev Modern Phys 2005;77(1):137–85.
[3] Strogatz SH. From Kuramoto to Crawford: exploring the onset of synchronization in populations of coupled oscillators. Physica D 2000;143(1):1–20.
[4] Glass L. Synchronization and rhythmic processes in physiology. Nature 2001;410:277.
[5] Strogatz SH. Exploring complex networks. Nature 2001;410:268.
[6] Strogatz SH. Nonlinear dynamics and chaos: With applications to physics, biology, chemistry and engineering. 2nd ed. Massachusetts: Westview Press; 2000, p. 512.
[7] Boccaletti S, Latora V, Moreno Y, Chavez M, Hwang D-U. Complex networks: Structure and dynamics. Phys Rep 2006;424(4):175–308.
[8] Estrada E. The structure of complex networks: theory and applications. 1st ed. United Kingdom: Oxford University Press; 2012.
[9] Sporns O, Chialvo DR, Kaiser M, Hilgetag C. Organization, development and function of complex brain networks. Trends in Cognitive Sciences 2004;8(9):418–25.
[10] Ferrari FAS, Viana RL, Reis AS, Iarosz KC, Caldas IL, Batista AM. A network of networks model to study phase synchronization using structural connection matrix of human brain. Phys A 2018;496:162–70.
[11] Lameu EL, Borges FS, Borges RR, Iarosz KC, Caldas IL, Batista AM, et al. Suppression of phase synchronisation in network based on cat's brain. Chaos 2016;26:043107.
[12] Batista CAS, Batista AM, de Pontes JAC, Viana RL, Lopes SR. Chaotic phase synchronization in scale-free networks of bursting neurons. Phys Rev E 2007;76(1):016218.
[13] Batista CAS, Batista AM, Pontes JCA, Lopes SR, Viana RL. Bursting synchronization in scale-free networks. Chaos Solitons Fractals 2009;41(5):2220–5.
[14] Lameu EL, Batista CAS, Batista AM, Iarosz KC, Viana RL, Lopes SR, et al. Suppression of bursting synchronization in clustered scale-free (rich-club) neuronal networks. Chaos 2012;22:043149.
[15] Protachevicz PR, Borges RR, Reis AS, Borges FS, Iarosz KC, Caldas IL, et al. Synchronous behaviour in network model based on human cortico-cortical connections. Physiol Meas 2018;39(7):074006.
[16] Hammond C, Bergman H, Brown P. Pathological synchronization in Parkinson's disease: networks, models and treatments. Trends Neurosci 2007;30(7):357–64.
[17] Schnitzler A, Munks C, Butz M, Timmermann L, Gross J. Synchronized brain network associated with essential tremor as revealed by magnetoencephalography. Mov Disord 2009;(24):1629–35.
[18] Frolov N, Grubov V, Maksimenko V, Lüttjohann A, Makarov VV, Pavlov AN, et al. Statistical properties and predictability of extreme epileptic events. Sci Rep 2019;9:7243.
[19] Karpov OE, Grubov VV, Maksimenko VA, Utaschev N, Semerikov VE, Andrikov DA, et al. Noise amplification precedes extreme epileptic events on human EEG. Phys Rev E 2021;103:022310.
[20] Koronovskii AA, Hramov AE, Grubov VV, Moskalenko OI, Sitnikova E, Pavlov AN. Coexistence of intermittencies in the neuronal network of the epileptic brain. Phys Rev E 2016;93:032220.
[21] Jiruska P, Curtis M, Jefferys JGR, Schevon CA, Schiff SJ, Schindler K. Synchronization and desynchronization in epilepsy: controversies and hypotheses. Physica D 2013;591(4):787–97.
[22] Bassett DS, Sporns O. Network neuroscience. Nature Neurosci 2017;20:353–64.
[23] Mugnaine M, Reis AS, Borges FS, Borges RR, Ferrari FAS, Iarosz KC, Caldas IL, Lameu E, Viana RL, Szezech JD, Kurths J, Batista AM. Delayed feedback control of phase synchronisation in a neuronal network model. Eur Phys J Spec Top 2018;227(10):1151–60.
[24] Batista CAS, Lameu EL, Lopes SR, Pereira T, Zamora-López G, Viana RL. Phase synchronization of bursting neurons in clustered small-world networks. Phys Rev E 2012;86:016211.
[25] Prado TL, Lopes SR, Batista CAS, Kurths J, Viana RL. Synchronization of bursting Hodgkin-Huxley-type neurons in clustered networks. Phys Rev E 2014;90:032818.
[26] Reis AS, Iarosz K, Ferrari FAS, Caldas IL, Batista AM, Viana RL. Bursting synchronisation in neuronal assemblies of scale-free networks. Chaos Solitons Fractals 2020;110395.
[27] Reis AS, Brugnago EL, Caldas IL, Batista AM, Iarosz KC, Ferrari F, et al. Suppression of chaotic bursting synchronization in clustered scale-free networks by an external feedback signal. Chaos 2021;31:083128.
[28] Hilgetag C-C, Burns GA, O'Neill MA, Scannell JW, Young MP. Anatomical connectivity defines the organization of clusters of cortical areas in the macaque and the cat. Philos Trans R Soc London [Biol] 2000;355(1393):91–110.
[29] Scannell J, Burns G, Hilgetag C, O'Neil M, Young M. The connectional organization of the cortico-thalamic system of the cat. Cerebral Cortex 1999;9(3):277–99.
[30] van den Heuvel M, Stam C, Boersma M, Hulshoff Pol H. Small-world and scale-free organization of voxel-based resting-state functional connectivity in the human brain. NeuroImage 2008;43(3):528–39.
[31] Eguiluz VM, Chialvo DR, Cecchi GA, Baliki M, Apkarian VA. Scale-free brain functional networks. Phys Rev Lett 2005;94:018102.
[32] Barabási A-L, Albert R. Emergence of scaling in random networks. Science 1999;286:507–12.
[33] Bianconi G, Barabási A-L. Competition and multiscaling in evolving networks. Europhys Lett 2001;54(4):436–42.
[34] Rulkov NF. Regularization of synchronized chaotic bursts. Phys Rev Lett 2001;86:183–6.
[35] Lo C-Y, Wang P-N, Chou K-H, Wang J, He Y, Lin C-P. Diffusion tensor tractography reveals abnormal topological organization in structural cortical networks in alzheimer's disease. J Neurosci 2010;30(50):16876–85.
[36] Kuramoto Y. Chemical oscillations, waves, and turbulence. 8th ed. Berlin: Springer-Verlag; 1984, p. 156.
[37] Arenas A, Díaz-Guilera A, Kurths J, Moreno Y, Zhou C. Synchronization in complex networks. Phys Rep 2008;469(3):93–153.

[38] Rosenblum MG, Pikovsky A. Delayed feedback control of collective synchrony: An approach to suppression of pathological brain rhythms. Phys Rev E 2004;70:041904.
[39] Rosenblum MG, Pikovsky A. Controlling synchronization in an ensemble of globally coupled oscillators. Phys Rev Lett 2004;92(11):102–14.
[40] Noback CR, Ruggiero DA, Demarest RJ, Strominger NL. The human nervous system: Structure and function. 6th ed. Totowa: Humana Press; 2005, p. 475.
[41] Winfree AT. Biological rhythms and the behavior of populations of coupled oscillators. J Theoret Biol 1967;16(1):15–42.
[42] Pyragas K. Delayed feedback control of chaos. Phil Trans R Soc A 2006;364(1846):2309–34.
[43] Gómez-Gardeñes J, Gómez S, Arenas A, Moreno Y. Explosive synchronization transitions in scale-free networks. Phys Rev Lett 2011;106:128701.